Monthly Notices
of the
ROYAL ASTRONOMICAL SOCIETY

Mon. Not. R. Astron. Soc. **408,** 133–138 (2010) doi:10.1111/j.1365-2966.2010.17222.x

High-velocity feature of the class I methanol maser in G309.38−0.13

M. A. Voronkov,[1,2★] J. L. Caswell,[1] T. R. Britton,[1,3] J. A. Green,[1] A. M. Sobolev[4] and S. P. Ellingsen[5]

[1]*Australia Telescope National Facility, CSIRO Astronomy and Space Science, PO Box 76, Epping, NSW 1710, Australia*
[2]*Astro Space Centre, Profsouznaya st. 84/32, 117997 Moscow, Russia*
[3]*Macquarie University, Department of Physics and Engineering, NSW 2109, Australia*
[4]*Ural State University, Lenin ave. 51, 620083 Ekaterinburg, Russia*
[5]*School of Mathematics and Physics, University of Tasmania, GPO Box 252-37, Hobart, Tasmania 7000, Australia*

Accepted 2010 June 2. Received 2010 June 1; in original form 2010 May 17

ABSTRACT

The Australia Telescope Compact Array (ATCA) has been used to map class I methanol masers at 36 and 44 GHz in G309.38−0.13. Maser spots are found at nine locations in an area of 50 × 30 arcsec^2, with both transitions reliably detected at only two locations. The brightest spot is associated with shocked gas traced by 4.5-μm emission. The data allowed us to make a serendipitous discovery of a high-velocity 36-GHz spectral feature, which is blueshifted by about 30 km s^{-1} from the peak velocity at this frequency, but spatially located close to (within a few arcseconds of) the brightest maser spot. We interpret this as indicating an outflow parallel to the line of sight. Such a high-velocity spread of maser features, which has not been previously reported in the class I methanol masers associated with a single molecular cloud, suggests that the outflow most likely interacts with a moving parcel of gas.

Key words: masers – ISM: jets and outflows – ISM: molecules.

1 INTRODUCTION

Methanol masers are commonly found in high-mass star-forming regions, with more than 20 different centimetre and millimetre wavelength masing transitions discovered to date (e.g. Müller et al. 2004). All methanol maser transitions do not share the same behaviour. Empirically, they form two classes (Batrla et al. 1987). Class I methanol masers (e.g. at 36, 44, 84 and 95 GHz) usually occur in multiple locations across the star-forming region scattered around an area up to a parsec in extent (e.g. Kurtz et al. 2004; Voronkov et al. 2006; Cyganowski et al. 2009). In contrast, class II methanol masers (e.g. at 6.7, 12 and 107 GHz) reside in the close vicinity of exciting young stellar objects (YSOs) and are typically found as a single cluster of emission at arcsecond resolution (e.g. Phillips et al. 1998). Theoretical calculations are able to explain this empirical classification and strongly suggest that the pumping process of class I masers is dominated by collisions with molecular hydrogen, in contrast to class II masers which are pumped by radiative excitation (e.g. Voronkov et al. 2005, and references therein).

The morphology of class I methanol masers has recently become the focus of high angular resolution studies aimed at searching for associations with other phenomena commonly observed in regions of high-mass star formation (e.g. Cyganowski et al. 2009). The common consensus is that the majority of class I masers trace interface regions between outflows and molecular gas, although direct observational evidence of this has been obtained for a limited number of sources only (e.g. Plambeck & Menten 1990; Kurtz et al. 2004; Voronkov et al. 2006). The alternative scenarios involving cloud–cloud collisions (e.g. Sobolev 1992; Salii, Sobolev & Kalinina 2002; Sjouwerman, Pihlström & Fish 2010) as well as the interaction of expanding HII regions with the ambient molecular environment (Voronkov et al. 2010) may also be realized in some sources. The common point of all these scenarios is the presence of shocked gas, where the physical conditions are favouring class I methanol masers (see the discussion in Section 4.1). Apart from the outflow associations cited above (based on the 2.12-μm H_2 emission, which is a well-known shock tracer), Cyganowski et al. (2009) reported association of some class I maser spots with the extended features showing a prominent excess of the 4.5-μm emission in the images obtained with the *Spitzer Space Telescope*'s Infrared Array Camera (IRAC), also known as extended green objects (EGOs; Cyganowski et al. 2009) or 'green fuzzies' (Chambers et al. 2009). The excess of the 4.5-μm (IRAC band 2) emission could be a result of shock excitation of molecular hydrogen and carbon monoxide in protostellar outflows (Chambers et al. 2009; Cyganowski et al. 2009; De Buizer & Vacca 2010). It is worth noting that Chen, Ellingsen & Shen (2009) demonstrated statistically the presence of an EGO in the vicinity of a large fraction of class I methanol masers at low angular resolution (single-dish positions). To increase the number of class I masers studied at high angular resolution and to compare the morphologies observed in different maser transitions, we carried out an interferometric survey at 36 and 44 GHz of all class I

★E-mail: Maxim.Voronkov@csiro.au

masers previously reported in the literature and located south of declination -35°. In this paper, we present a study of G309.38−0.13, an especially interesting source from the survey. It represents the level of morphological and kinematical complexity encountered for the majority of sources observed in the survey, but it has a distinct high-velocity maser feature at 36 GHz, which was quite unexpected (see e.g. Bachiller et al. 1990; Kalenskii et al. 2010). This maser is found in an area devoid of bright radio-continuum emission, but near-infrared sources which are presumably embedded stars. It is located approximately 20 arcmin offset from the prominent H II region Gum 48d at the heliocentric distance of about 3.5 kpc (for further information on the region see Karr, Manoj & Ohashi 2009).

2 OBSERVATIONS

Observations were made with the Australia Telescope Compact Array (ATCA) in 2007 May as part of the interferometric survey of southern class I methanol masers at 36 and 44 GHz (project code C1642). The source was observed using the hybrid H214C array configuration in a few 3-min cuts (four cuts at 36 GHz and six at 44 GHz) spread in hour angle for better *uv* coverage. We did not use, for imaging, the data from the CA06 antenna (located about 4.5 km to the west of the other five antennas). The remaining antennas provided baselines ranging from 82 to 240 m. The position of the phase and pointing centre was $\alpha_{2000} = 13^{\rm h}47^{\rm m}26\overset{\rm s}{.}01$, $\delta_{2000} = -62^\circ 18' 11\overset{''}{.}66$. We used reference-pointing procedures and determined corrections using the continuum source 1414-59 (which served also as a phase calibrator). From the statistics of pointing solutions, the reference-pointing accuracy was estimated to be 4.8 ± 2.6 arcsec. This accuracy affects the accuracy of flux-density measurements, particularly for sources of emission which are offset from the pointing centre. The positional accuracy of the maser locations depends on the quality of the phase calibration and is believed to be better than 0.5 arcsec. The absolute flux-density scale was bootstrapped from observation of Uranus (assumed flux densities were 1.38 and 1.98 Jy at 36 and 44 GHz, respectively). We estimate the flux scale to be accurate to about 20 per cent. The correlator was configured to split 8-MHz bandwidth into 1024 spectral channels. The resulting spectral resolution and velocity range covered are given in Table 1 along with other observing parameters. Most columns of Table 1 are self-explanatory and include, in addition to above, the molecular transition and its rest frequency (adopted from Müller et al. 2004), full width at half-maximum (FWHM) and position angle (PA) of the synthesized beam reflecting the spatial resolution, as well as the size of the primary beam which determines the field of view. The 1σ rms noise given in the seventh column is a median value of rms noise levels obtained for each individual spectral plane of the image cube prior to the primary beam correction (i.e. with constant noise across the field of view). Scaled up with the primary beam, it represents the 1σ detection limit of these observations at a particular location. It is worth mentioning, however, that the ability to detect weak features is notably reduced within the velocity range of strong emission due to dynamic range limitations, which were largely a result of sparse *uv* coverage. We estimate the dynamic range (the ratio of peak flux to rms noise in the image) to be about 90 and 400 for the 36- and 44-GHz image cubes, respectively. The uncertainty of the radial velocity corresponding to the rest-frequency uncertainty is given in the ninth column of Table 1.

Data reduction in MIRIAD followed the standard procedure including an opacity correction based on the model built into MIRIAD and atmospheric temperature, pressure and humidity registered at the time of observations by the ATCA weather station. We used uniform weighting for the imaging. After absolute positions had been determined we performed self-calibration (solution interval 1 min) using the brightest spectral feature as a reference. The flux-density ratio of the reference feature before and after self-calibration allowed us to estimate decorrelation caused by atmospheric phase variations occurring on a time-scale shorter than 5 min, the minimum temporal separation from the secondary calibrator scan. We estimated decorrelation factors to be 1.18 ± 0.01 and 1.03 ± 0.02 at 44 and 36 GHz, respectively. The full velocity range was imaged using the self-calibrated data set. Therefore, to first order, the effect of the atmospheric phase stability on the derived flux densities had been corrected for. The residual uncertainty is expected to be small compared to the accuracy of the flux-scale calibration. The maser emission was searched in the cube prior to the primary beam correction (i.e. the noise across the field of view was constant). Then, the cube was divided by the primary beam model at the appropriate frequency and the spectra were extracted at the peak pixel by taking a slice along the spectral axis. We followed this approach due to the rather high side lobe level in the point spread function caused by the poor *uv*-coverage attained in the project. It reproduces flux density correctly in the case of unresolved or barely resolved sources (i.e. smaller than the synthesized beam) and is well suited to maser observations.

3 RESULTS

The morphology of the region is shown in Fig. 1. The methanol emission is confined to nine discrete locations, labelled A−I, spread over a 50 × 30-arcsec^2 region. The spectra at most locations are complex, consisting of more than one spectral feature (Fig. 2). At finer scale (less than the synthesized beam size), each spectral feature corresponds to a slightly different position in the map. Most of the features are believed to be spots of class I maser emission for reasons summarized at the end of this section. E is at essentially the same position as B, but was designated by a separate letter as it corresponds to a distinct group of velocities, blueshifted by approximately 30 km s^{-1}. We show the positions of all spectral features corresponding to each spot (circles denote the brightest feature, crosses show all other features) in Fig. 1 along with the

Table 1. Observation details. The rms noise is calculated as a median of the noise levels obtained for each spectral plane of the image cube prior to the primary beam correction. The velocity uncertainty corresponds to the uncertainty of the rest frequency, which is given in the brackets following the value of the rest frequency and is expressed in the units of the least significant figure.

Molecular transition	UT date of observation	Rest frequency (MHz)	Synthesized beam FWHM (arcsec)	Synthesized beam PA (°)	Primary beam FWHM (arcmin)	1σ rms noise (mJy)	Velocity range (km s^{-1})	Velocity uncertainty (km s^{-1})	Spectral resolution (km s^{-1})
$4_{-1} - 3_0$ E	2007 May 23	36 169.265 (30)	6.0 × 4.7	76	1.40	100	−85.4, −26.0	0.24	0.066
$7_0 - 6_1$ A$^+$	2007 May 22	44 069.410 (10)	5.3 × 4.0	80	1.15	130	−76.9, −28.3	0.068	0.054

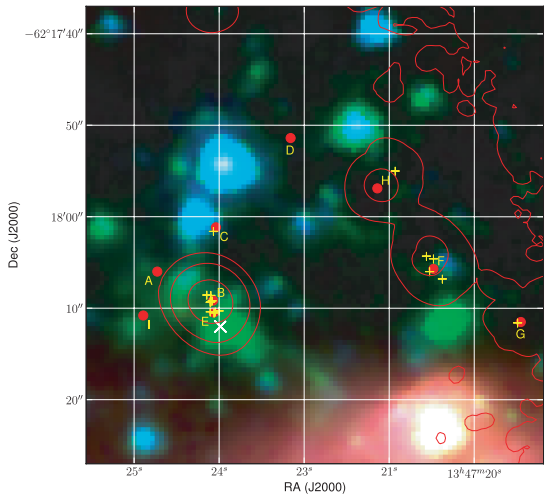

Figure 1. Positions of class I methanol masers (red filled circles and yellow crosses) overlaid on top of the three-colour *Spitzer* image of the G309.38−0.13 region. The emission in 8.0-, 4.5- and 3.6-μm IRAC *Spitzer* bands is shown as red, green and blue, respectively. The filled red circles show the fitted position of the strongest spectral component at each location, while the weaker components are shown by yellow crosses (all components are given in Table 2). The location of a class II 6.7-GHz methanol maser (Caswell 2009) is shown by the white cross. The contours show the maximum of the 36-GHz emission across all spectral channels. The levels are 5, 15, 50 and 90 per cent of the peak 36-GHz flux density of 16.1 Jy. Low-level artefacts in the top right-hand corner are caused by the primary beam correction.

position of the class II methanol maser at 6.7 GHz (Caswell 2009). The 6.7-GHz maser in this region peaks at $-49.6\,\mathrm{km\,s^{-1}}$ and is quite weak (1 Jy). It is found at $\alpha_{2000} = 13^{\mathrm{h}}47^{\mathrm{m}}23\overset{\mathrm{s}}{.}98$, $\delta_{2000} = -62^{\circ}18'12\overset{''}{.}0$, just a few seconds of arc south of the class I maser emission at B and E. Both the OH and H_2O masers are, within the measurement uncertainty, at the same position as the 6.7-GHz maser and have radial velocities near $-50\,\mathrm{km\,s^{-1}}$ (Caswell 1998; Breen et al. 2010). The three-colour background in Fig. 1 shows the emission in the 8.0-, 4.5- and 3.6-μm IRAC *Spitzer* bands as red, green and blue, respectively. The infrared image reveals an EGO in the vicinity of B and E, which is likely to be a signature of the shocked gas. A number of compact sources showing excess in the 4.5-μm band (appearing green in Fig. 1) are also present. In particular, such a source is located near F and G.

The spectra at all locations except I are shown in Fig. 2. The latter is not shown due to a poor signal-to-noise ratio, but qualified as a detection due to its isolation in velocity from the other bright emission in the region, despite being comparable in flux density to dynamic range artefacts seen at other velocities. Only B and F were reliably detected at both 36 and 44 GHz. E, G and H were detected at 36 GHz only, while only 44-GHz emission was detected at A, C, D and I. To describe individual spectral features, we decomposed the spectra into a number of Gaussian components (the sum of the components represents each spectrum within measurement errors). The local standard of rest (LSR) velocity, position, velocity FWHM of the component and the flux density are given on the left-hand side of Table 2. The position fit was done assuming a point source model, typically at the peak velocity for the appropriate component. In the case of significant blending, the position fit is expected to have a systematic error and give a flux-density-weighted average position of the blended Gaussian components. We estimate that the systematic errors of the fitted position are likely to be less than the random errors of the fit given in Table 2 for most components in this particular source. Two exceptions are the 30-Jy component towards B at 44 GHz and the $-78.6\,\mathrm{km\,s^{-1}}$ component towards E. Both were fitted with a single Gaussian component, although the profile shape in Fig. 2 suggests that at least two independent components may be present in each case.

The relatively compact ATCA configuration used for observations allows us to put only a relatively weak constraint on the brightness temperature (>100 K), which is insufficient to prove the maser nature of the observed emission unambiguously. However, given the linewidth of the majority of components (Table 2 and Fig. 2), at least some of the emission is likely to be due to maser action for most of the features. In addition, we verified that the dominant emission at both B (at both frequencies) and E is unresolved at baselines to distant CA06 antenna, which implies brightness temperatures exceeding 10^6 K, and, therefore, a maser origin of this emission. The right-hand side of Table 2 shows the parameters of the line profile at each maser location, such as the LSR velocity and the flux density of the peak as well as the integral over the line profile.

4 DISCUSSION

4.1 High-velocity maser feature

The blueshifted spectral component corresponding to location E is a remarkable feature of this maser source. More commonly, the observed velocities of class I methanol masers are no more than a few $\mathrm{km\,s^{-1}}$ from the velocity of the ambient molecular cloud, and the velocity dispersion is low (e.g. Bachiller et al. 1990; Plambeck & Menten 1990; Voronkov et al. 2006; Araya et al. 2009). The notable exception with a high velocity dispersion is G1.6−0.025, which has emission components at radial velocities ranging from 0 to $160\,\mathrm{km\,s^{-1}}$ (Haschick & Baan 1993; Salii et al. 2002). However, unlike G309.38−0.13, the emission in G1.6−0.025 corresponds to distinct, but interacting, molecular clumps detected also in a number of thermal transitions of various molecules (Salii et al. 2002). The large velocity difference between individual clumps reflects a violent environment and the exceptional kinematics in the vicinity of the Galactic Centre.

In contrast, the G309.38−0.13 region is close to the tangential direction of the Sagittarius–Carina Arm (see fig. 5 of Russeil 2003) where the extreme velocity of E ($-80\,\mathrm{km\,s^{-1}}$) makes an association with an unrelated molecular cloud highly unlikely. This is corroborated by the ^{12}CO brightness temperature limit of 0.1 K at the radial velocities below $-70\,\mathrm{km\,s^{-1}}$ obtained with the 4-m Nanten telescope (Saito et al. 2001). This limit is two orders of magnitude lower than the peak ^{12}CO brightness temperature observed near $-50\,\mathrm{km\,s^{-1}}$ in the G309.38−0.13 region (nearest ^{18}CO clump mass is about $10^4\,\mathrm{M_\odot}$; Saito et al. 2001), which is close to the velocities of most of the maser spots.

We conclude that the high-velocity 36-GHz maser in E most likely reflects the presence of a molecular outflow, rather than a separate molecular cloud projecting on to the same location by chance. The area around B and E is characterized by the presence of shocked gas traced by a strong EGO (Fig. 1). This supports the idea that an outflow is present. The close spatial location of B and E and the presence of the class II methanol maser (which indicates the presence of a high-mass YSO) in the vicinity both suggest that the outflow axis is close to the line of sight.

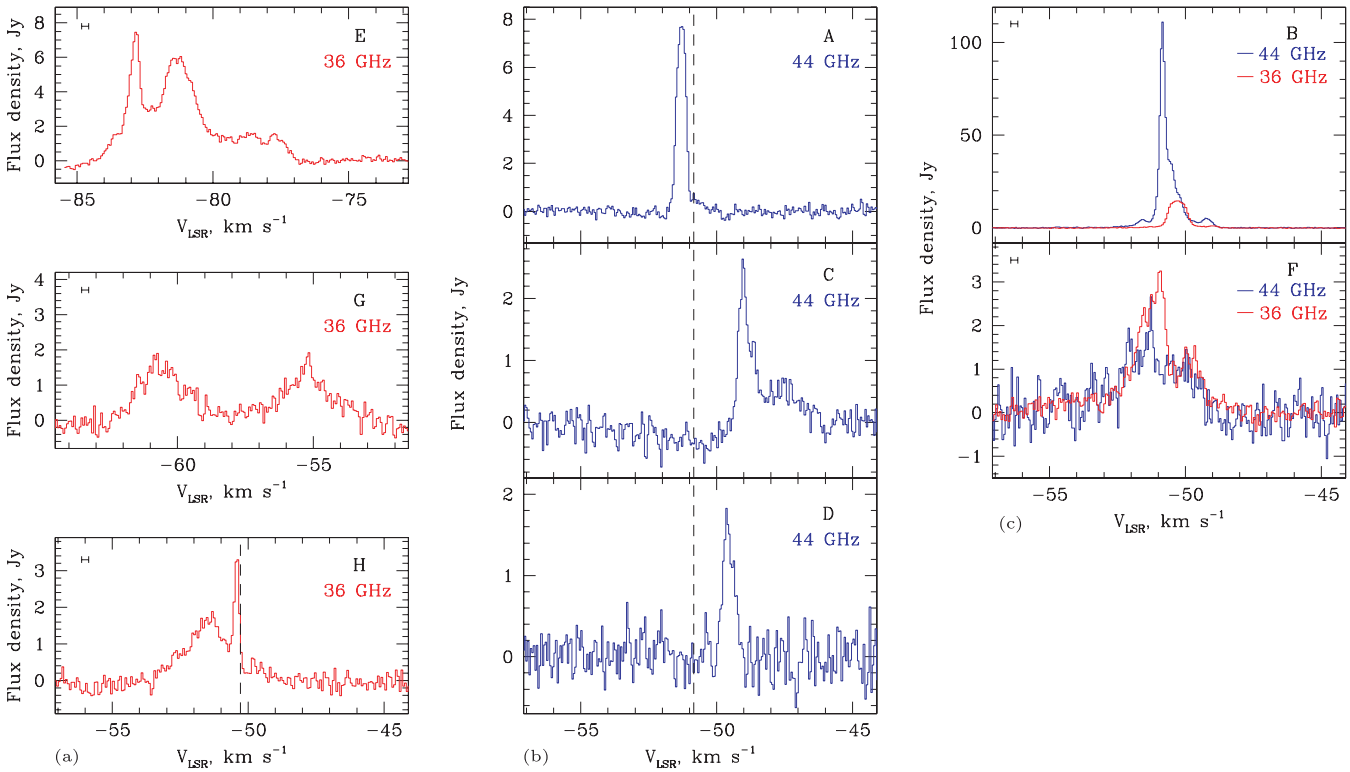

Figure 2. Spectra of the 36-GHz (red) and 44-GHz (blue) emission at eight locations in G309.38−0.13 (location I is not shown here due to low signal-to-noise ratio in the spectrum). The dashed line shows the peak velocity of the brightest spectral feature (at location B) at the given frequency. (a) Emission from E (high-velocity feature), G and H was detected at 36 GHz only. (b) A, C and D were detected at 44 GHz only. (c) B (main feature) and F were detected at both 36 and 44 GHz. The uncertainty of the relative velocity alignment between transitions is dominated by the rest-frequency uncertainty of the 36-GHz transition shown by the horizontal error bar in spectra showing 36-GHz emission (it is comparable to the spectral resolution for the 44-GHz transition).

As mentioned earlier, the interaction between outflows and the ambient material is believed to be responsible for the majority of class I methanol masers. The production of methanol by purely gas-phase chemical reactions is quite inefficient, but the passage of weak shocks is expected to release methanol from the grain mantles (e.g. Hartquist et al. 1995). Enhanced methanol abundance arising from shocks driven by outflows into the ambient cloud has also been confirmed observationally (e.g. Gibb & Davis 1998; Garay et al. 2002). In addition, outflows compress the medium, which makes collisions more frequent and the pumping mechanism more efficient. However, methanol is expected to survive sputtering and desorption of grain mantles only if the shocks are relatively mild, i.e. at shock velocities not greatly exceeding 10 km s^{-1} (Garay et al. 2002). Therefore, the detection of a maser feature offset by 30 km s^{-1} with respect to the velocity of the ambient gas is somewhat surprising.

This discrepancy can be resolved if the outflow interacts with a moving parcel of gas. In this case, the same radial velocity of the maser can be achieved for a lower shock velocity. The mechanism of this gas acceleration is unknown at present. It could be by a previous outflow event or a different outflow from another YSO. In addition, the clustered environment of high-mass star formation opens a range of possibilities for gravitational acceleration of gas clumps (e.g. mechanisms which caused radial velocity outliers observed in clusters of low-mass protostars by Covey et al. 2006). One may speculate that the curved morphology of the EGO associated with B and E (Fig. 1) suggests interaction with an outflow coming from the south-west (the general direction of the HII region Gum 48d). This may be the additional outflow responsible for the unusual kinematics. However, the distance of Gum 48d is estimated to be 3.5 kpc (Karr et al. 2009), and therefore Gum 48d must be at least 20 pc away from the maser. A separation of the terminal shock from the driving source as large as this is unprecedented (e.g. the outflow studied by Brooks et al. 2003 extends only up to 1.5 pc) and suggests that, if the EGO is indeed shaped by the second outflow, the driving source is not the star responsible for the excitation of Gum 48d.

4.2 Relative flux density of 36- and 44-GHz methanol masers

An inspection of Table 2 and Fig. 2 suggests that the 36- to 44-GHz flux-density ratio varies significantly from component to component. The majority of maser features were detected in a single transition only and most striking is the lack of a 36-GHz counterpart to the brightest 44-GHz spectral feature (Fig. 2c). Although the velocities corresponding to E (high-velocity feature) were not covered by the 44-GHz measurement, the preliminary results of a follow-up observation carried out with the Mopra 22-m single dish in 2010 January showed no 44-GHz methanol (as well as no 48-GHz methanol, SiO 1–0 and CS 1–0) emission near −80 km s^{-1} above 1.3 Jy. With the caveat about possible temporal variability over the 2.5-yr time-scale, this situation represents another extreme case of a 36-GHz maser without a 44-GHz counterpart. The numerical models of Sobolev et al. (2005) suggest that the 44-GHz masers are quite sensitive to the geometry of the maser region. Unlike 36-GHz masers, which can be produced in the spherically symmetric case, an optical depth along the line of sight higher than in the orthogonal direction seems to be the key property required to produce bright 44-GHz masers. One could expect this elongation of the gas clumps

Table 2. Fit results and profile parameters. The uncertainties are given in parentheses and expressed in units of the least significant figure.

Spot	Molecular transition	Frequency (GHz)	Gaussian components: LSR velocity[a] (km s^{-1})	α_{2000} 13^h47^m (^{s})	δ_{2000} -62° (arcmin arcsec)	Line FWHM (km s^{-1})	Flux density (Jy)	Peak LSR velocity[b] (km s^{-1})	Peak flux density (Jy)	$\int f(v)\,dv$ (Jy km s^{-1})
A	$7_0 - 6_1$ A$^+$	44	−51.30	24.97 (2)	18 06.0 (1)	0.387 (3)	7.90 (6)	−51.27	7.6 (2)	3.21 (3)
B	$4_{-1} - 3_0$ E	36	−51.34	24.0 (1)	18 10.3 (6)	0.42 (6)	1.0 (1)	−50.31	14.6 (1)	12.41 (3)
			−50.295	24.141 (7)	18 09.35 (4)	0.715 (5)	15.96 (9)			
			−49.06	24.13 (3)	18 08.6 (2)	0.55 (6)	1.1 (1)			
	$7_0 - 6_1$ A$^+$	44	−51.6	24.13 (3)	18 09.3 (2)	0.5 (3)	3.5 (2)	−50.84	111.1 (2)	50.82 (6)
			−50.851	24.095 (2)	18 09.165 (8)	0.192 (1)	85.9 (3)			
			−50.58	24.110 (4)	18 09.02 (2)	0.78 (3)	30.7 (7)			
			−49.23	24.194 (8)	18 08.56 (4)	0.6 (2)	4.4 (9)			
C	$7_0 - 6_1$ A$^+$	44	−49.01	24.05 (2)	18 01.16 (9)	0.51 (3)	1.95 (7)	−49.04	2.6 (2)	2.12 (9)
			−47.83	24.09 (9)	18 01.6 (4)	1.7 (2)	0.49 (4)			
D	$7_0 - 6_1$ A$^+$	44	−49.57	22.88 (2)	17 51.4 (2)	0.55 (3)	1.54 (7)	−49.64	1.8 (3)	0.81 (2)
E	$4_{-1} - 3_0$ E	36	−83.50	24.14 (3)	18 10.4 (2)	0.75 (5)	1.49 (9)	−82.84	7.5 (2)	18.27 (8)
			−82.854	24.085 (8)	18 10.47 (5)	0.485 (9)	6.5 (1)			
			−81.33	24.080 (3)	18 10.52 (2)	1.64 (2)	6.5 (1)			
			−78.60	24.06 (3)	18 10.4 (2)	2.28 (9)	1.44 (5)			
F	$4_{-1} - 3_0$ E	36	−52.0	20.64 (8)	18 05.7 (5)	5.0 (3)	0.51 (2)	−50.92	3.3 (2)	5.49 (2)
			−51.07	20.64 (5)	18 04.6 (3)	1.33 (2)	2.66 (4)			
			−49.66	20.75 (4)	18 04.3 (3)	0.67 (4)	1.12 (5)			
	$7_0 - 6_1$ A$^+$	44	−51.76	20.5 (2)	18 06.8 (7)	1.35 (9)	1.26 (7)	−51.27	2.7 (4)	3.5 (2)
			−49.62	20.7 (2)	18 06 (1)	1.1 (2)	0.57 (8)			
G	$4_{-1} - 3_0$ E	36	−60.56	19.27 (5)	18 11.5 (3)	1.98 (8)	1.54 (6)	−55.16	1.9 (4)	7 (1)
			−55.29	19.32 (4)	18 11.6 (3)	2.2 (1)	1.31 (5)			
H	$4_{-1} - 3_0$ E	36	−51.50	21.24 (3)	17 55.0 (2)	2.04 (5)	1.48 (3)	−50.39	3.3 (2)	3.79 (5)
			−51.432	21.52 (2)	17 56.9 (1)	0.275 (8)	3.30 (9)			
I	$7_0 - 6_1$ A$^+$	44	−53.25	25.19 (5)	18 10.8 (2)	0.81 (8)	0.43 (4)	−53.29	0.6 (2)	0.404 (8)

[a]The uncertainty is half of that for the line FWHM.
[b]The uncertainty is the spectral resolution listed in Table 1.

involved in the maser action to be somehow related to the outflow orientation and morphology. However, the complexity of the maser spot distribution (see Fig. 1) does not allow us to interpret the flux-density ratios for each spot in a consistent manner based on just the spot location with respect to the suspected outflow (the position of the 6.7-GHz maser presumably marks the location of the YSO driving the outflow roughly along the line of sight).

5 CONCLUSIONS

(i) Spots of class I methanol maser emission in G309.38−0.13 are spread over an area of 50 × 30 arcsec^2 in extent (see Table 2 and Fig. 1). Both 36- and 44-GHz maser emission was detected at two locations, while the emission from the remaining locations was detected at a single frequency only (see Fig. 2).

(ii) We report the detection of a high-velocity spectral feature at 36 GHz, blueshifted by about 30 km s^{-1} from the peak velocity. This is the largest velocity offset reported so far for a class I methanol maser source associated with a single molecular cloud. The maser corresponding to this feature (labelled E) is located within a few seconds of arc of the maser at B (the brightest spectral feature at both frequencies) indicating a possible association with an outflow parallel to the line of sight.

(iii) The results highlight the importance of not only high spectral and spatial resolution for studies of class I methanol masers, but also ample velocity coverage and a field of view wider than the typical primary beam size of available instruments. All observational data gathered so far lack at least one (and sometimes all) of these properties. In addition, the results show that the 36- and 44-GHz transitions are very complementary to each other. The high-velocity spectral feature in G309.38−0.13 is a good example of a phenomenon which has been missed by previous maser surveys.

ACKNOWLEDGMENTS

The Australia Telescope is funded by the Commonwealth of Australia for operation as a National Facility managed by CSIRO. SPE thanks the Alexander-von-Humboldt-Stiftung for an Experienced Researcher Fellowship which has helped support this research. AMS was financially supported by the Russian Foundation for Basic Research (grant 10-02-00589-a) and the Russian federal programme 'Scientific and scientific-pedagogical personnel of innovational Russia' (contracts 02.740.11.0247 from 07.07.2009 and 540 from 05.08.2009). The research has made use of the NASA/IPAC Infrared Science Archive, which is operated by the Jet Propulsion Laboratory, California Institute of Technology, under contract with the National Aeronautics and Space Administration.

REFERENCES

Araya E. D., Kurtz S., Hofner P., Linz H., 2009, ApJ, 698, 1321
Bachiller R., Menten K. M., Gómez-González J., Barcia A., 1990, A&A, 240, 116
Batrla W., Matthews H. E., Menten K. M., Walmsley C. M., 1987, Nat, 326, 49
Breen S. L., Caswell J. L., Ellingsen S. P., Phillips C. J., 2010, MNRAS, in press (arXiv:1004.1060) (doi:10.1111/j.1365-2966.2010.16791.x)

Brooks K. J., Garay G., Mardones D., Bronfman L., 2003, ApJ, 594, 131
Caswell J. L., 1998, MNRAS, 297, 215
Caswell J. L., 2009, Publ. Astron. Soc. Australia, 26, 454
Chambers E. T., Jackson J. M., Rathborne J. M., Simon R., 2009, ApJS, 181, 360
Chen X., Ellingsen S. P., Shen Z. Q., 2009, MNRAS, 396, 1603
Covey K. R., Greene T. P., Doppmann G. W., Lada C. J., 2006, ApJ, 131, 512
Cyganowski C. J., Brogan C. L., Hunter T. R., Churchwell E., 2009, ApJ, 702, 1615
De Buizer J. M., Vacca W. D., 2010, AJ, 140, 196
Garay G., Mardones D., Rodriguez L. F., Caselli P., Bourke T. L., 2002, ApJ, 567, 980
Gibb A. G., Davis C. J., 1998, MNRAS, 298, 644
Hartquist T. W., Menten K. M., Lepp S., Dalgarno A., 1995, MNRAS, 272, 184
Haschick A. D., Baan W. A., 1993, ApJ, 410, 663
Kalenskii S. V., Johansson L. E. B., Bergman P., Kurtz S., Hofner P., Walmsley C. M., Slysh V. I., 2010, MNRAS, 405, 613
Karr J. L., Manoj P., Ohashi N., 2009, ApJ, 697, 133
Kurtz S., Hofner P., Álvarez C. V., 2004, ApJS, 155, 149
Müller H. S. P., Menten K. M., Mäder H., 2004, A&A, 428, 1019
Phillips C. J., Norris R. P., Ellingsen S. P., McCulloch P. M., 1998, MNRAS, 300, 1131
Plambeck R. L., Menten K. M., 1990, ApJ, 364, 555
Russeil D., 2003, A&A, 397, 133
Saito H., Mizuno N., Morigichi Y., Matsunaga K., Onishi T., Mizuno A., Fukui Y., 2001, PASJ, 53, 1037
Salii S. V., Sobolev A. M., Kalinina N. D., 2002, Astron. Rep., 46, 955
Sjouwerman L. O., Pihlström Y. M., Fish V. L., 2010, ApJ, 710, L111
Sobolev A. M., 1992, SvA, 36, 590
Sobolev A. M., Ostrovskii A. B., Kirsanova M. S., Shelemei O. V., Voronkov M. A., Malyshev A. V., 2005, in Churchwell E., Conti P., Felli M., eds, Proc. IAU Symp. 227, Massive Start Birth: A Crossroads of Astrophysics. Cambridge Univ. Press, Cambridge, p. 174
Voronkov M. A., Sobolev A. M., Ellingsen S. P., Ostrovskii A. B., 2005, MNRAS, 362, 995
Voronkov M. A., Brooks K. J., Sobolev A. M., Ellingsen S. P., Ostrovskii A. B., Caswell J. L., 2006, MNRAS, 373, 411
Voronkov M. A., Caswell J. L., Ellingsen S. P., Sobolev A. M., 2010, MNRAS, 405, 2471

This paper has been typeset from a TEX/LATEX file prepared by the author.